Structure and radiation effect of Er-stuffed pyrochlore Er2(Ti2−xErx)O7−x/2 (x = 0–0.667)

ARTICLE *in* NUCLEAR INSTRUMENTS AND METHODS IN PHYSICS RESEARCH SECTION B BEAM INTERACTIONS WITH MATERIALS AND ATOMS · AUGUST 2015

Impact Factor: 1.12 · DOI: 10.1016/j.nimb.2015.04.058

Nuclear Instruments and Methods in Physics Research B 356-357 (2015) 69–74

Contents lists available at ScienceDirect

Nuclear Instruments and Methods in Physics Research B

journal homepage: www.elsevier.com/locate/nimb

Structure and radiation effect of Er-stuffed pyrochlore $Er_2(Ti_{2-x}Er_x)O_{7-x/2}$ (x = 0–0.667)

D.Y. Yang [a], C.P. Xu [a], E.G. Fu [b], J. Wen [a], C.G. Liu [a], K.Q. Zhang [a], Y.Q. Wang [c], Y.H. Li [a,*]

[a] School of Nuclear Science and Technology, Lanzhou University, Lanzhou 730000, China
[b] School of Physics, Peking University, Beijing 100871, China
[c] Materials Science and Technology Division, Los Alamos National Laboratory, Los Alamos, NM 87545, USA

ARTICLE INFO

Article history:
Received 27 February 2015
Received in revised form 23 April 2015
Accepted 23 April 2015

Keywords:
Stuffed pyrochlore
Ion irradiation
Amorphization
Lattice swelling

ABSTRACT

Er-stuffed pyrochlore series $Er_2(Ti_{2-x}Er_x)O_{7-x/2}$ (x = 0, 0.162, 0.286, 0.424 and 0.667) were synthesized using conventional ceramic processing procedures. The structure of $Er_2(Ti_{2-x}Er_x)O_{7-x/2}$ is effectively tailored by the Er stuffing level (x). In order to study the radiation effect of Er-stuffed pyrochlores, irradiation experiments were performed with 400 keV Ne^{2+} ions to fluences ranging from 5×10^{14} to 3.0×10^{15} ions/cm^2 at cryogenic condition. Irradiation induced microstructural evolution was examined using a grazing incidence X-ray diffraction technique. It is found that the irradiated layer of $Er_2(Ti_{2-x}Er_x)O_{7-x/2}$ undergoes significant lattice disordering and swelling at fluences of $\leqslant 1.5 \times 10^{15}$ ions/cm^2 and amorphization at fluences of $\geqslant 1.5 \times 10^{15}$ ions/cm^2. The radiation effect depends strongly on the chemical compositions of the samples. Both the lattice swelling percentage and the amorphous fraction decrease with increasing x. The experimental results are discussed in the context of cation antisite defect. The defect formation energy which varies as a function of x is responsible for the difference in the structural behaviors of $Er_2(Ti_{2-x}Er_x)O_{7-x/2}$ under 400 keV Ne^{2+} ion irradiation.

1. Introduction

Recently, there has been great interest in using materials with fluorite and fluorite-related structures, such as pyrochlore, as potential host phases for the immobilization of actinides, particularly Pu, produced in nuclear power plants [1,2]. The advantage of using pyrochlore as a potential waste form is that it possesses remarkable compositional diversity, structural flexibility, and chemical durability [1]. The structure of ordered stoichiometric $A_2B_2O_7$ pyrochlore belongs to $Fd\bar{3}m$ space group and is a superstructure of the ideal fluorite structure (AX_2). The difference is that there are two cation sites and one-eighth of unoccupied anion sites. The A cation is eight coordinated and located within a distorted cubic coordination polyhedron; the B cation is six coordinated and located within a distorted octahedron. The anion "vacancies" are ordered on the anion sublattice [3,4]. The stability of the pyrochlore structure is governed by the ratio of the ionic radii of A and B cations (r_A/r_B), which extends from 1.46 for $Gd_2Zr_2O_7$ to 1.78 for $Sm_2Ti_2O_7$ [4]. For $r_A/r_B > 1.78$, a monoclinic structure forms, whereas for $r_A/r_B < 1.46$, a defective fluorite structure forms.

Due to potential applications in immobilization of actinides, the performance of pyrochlores in extreme environments has been investigated in great detail [5–9]. Extensive irradiation studies have simulated α-decay damage induced by incorporated actinides in a wide variety of pyrochlore compositions using ion-beam irradiation in a broad energy range [10–12]. Radiation induces significant microstructural changes in pyrochlores, including amorphization [6,13], interstitial point-defect clustering, vacancy induced cavitation and concomitant swelling [14,15] and precipitation of new crystalline phases. As a result, the chemical and physical durability of the waste forms are severely affected, which can deteriorate their long-term performance. Combined with experimental results, theoretical studies [16,17] based on density functional theory and molecular dynamics have suggested that the 48*f* (Wyckoff notation) oxygen deviation parameter, A^{3+} and B^{4+} cation radius ratio, bond type and electron configuration should be considered to clarify the radiation tolerance of the materials. Lian et al. [7] have found that ion irradiation induces order-to-disorder (O-D) transition in pyrochlores is from an ordered pyrochlore structure to a disordered defective fluorite structure. More specifically, their further study has revealed that

* Corresponding author.
E-mail address: liyuhong@lzu.edu.cn (Y.H. Li).

http://dx.doi.org/10.1016/j.nimb.2015.04.058
0168-583X/

the pyrochlores which are more prone to undergo O-D transition are more resistant to radiation induced amorphization [6].

According to the phase diagrams of the A_2O_3–TiO_2 (A = Dy–Lu) systems, the pyrochlore phase in these systems has rather broad homogeneity ranges [18,19]. The pyrochlore structure remarkably displays a wide range of behavior in response to ion irradiation as a function of composition. As in the case of $Gd_2Zr_{2-x}Ti_xO_7$, a systematic increase in resistance to ion induced amorphization with increasing Zr content has been observed [20,21]. Therefore, it makes great sense to understand the effect of chemical composition on the radiation behavior of A_2O_3–TiO_2 binary systems. In present work, we have investigated the microstructural evolution of the stuffed titanate pyrochlore $Er_2(Ti_{2-x}Er_x)O_{7-x/2}$ (x = 0–0.667) series under 400 keV Ne^{2+} irradiation. We abbreviate $Er_2(Ti_{2-x}Er_x)O_{7-x/2}$ as ETO for simplicity in this paper.

2. Experimental

Polycrystalline ETO pellets, with x = 0, 0.162, 0.286, 0.424 and 0.667, were synthesized using conventional ceramic processing procedures from rare earth oxides Er_2O_3 (99.99% pure) and anatase TiO_2 (99.99% pure) as starting materials. The measured densities of sintered pellets were larger than ~90% of the theoretical density. Samples were finally polished to a mirror finish using W0.25 Diamond suspension.

Ion irradiations were carried out at cryogenic condition (~77 K) in the Ion Beam Materials Laboratory at Los Alamos National Laboratory, using a 200 kV Danfysik High Current Research Ion Implanter. The 400 keV Ne^{2+} ions were implanted at normal incidence to ion fluences ranging from 5×10^{14} to 3×10^{15} ions/cm^2. The displacement damage and projectile depth profile of the 400 keV Ne^{2+} ions in $Er_2Ti_2O_7$ were estimated using the Monte Carlo code SRIM [22], where the threshold displacement energies of Er, Ti and O are all arbitrarily assumed as 40 eV. The simulated displacement damage and Ne ion concentration for the fluence of 1.0×10^{15} ions/cm^2 are plotted in Fig. 1. The projected Ne^{2+} ion range is approximately 0.49 μm, whereas the irradiation peak damage range is approximately 0.38 μm. These estimated values were used for all compositions owing to their same constituent atoms and similar densities.

Irradiated samples were characterized using grazing incidence X-ray diffraction (GIXRD). The GIXRD measurements were performed using a Rigaku D/Max-2400 X-ray Diffractometer employing Cu-K_α radiation. The X-ray glancing incident angle α was 1°, at which the X-ray penetration range was approximately 0.21 μm [23], as showed in Fig. 1. Thus it is believed that the measurement characterized only the irradiated region near the sample surface. The range of 2θ was from 10° to 70°, the scan step was 0.02° and a dwell time of one second per step.

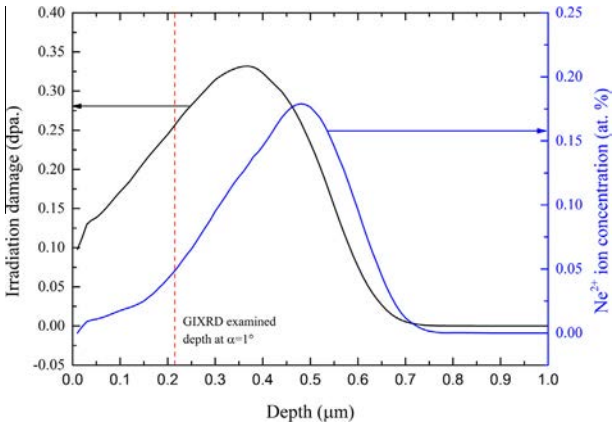

Fig. 1. The SRIM simulated irradiation damage and ion profile for 400 keV Ne implanting on $Er_2Ti_2O_7$ at a fluence of 1×10^{15} ions/cm^2.

3. Results and discussion

3.1. The structure of the pristine ETO

Fig. 2 shows the normalized profiles of XRD patterns of the five pristine samples sintered at 1500 °C. The intensity of each pattern was normalized with respect to the most intense diffraction peak at $2\theta \sim 31°$. The miller indices {hkl} of each peak were labeled in the figure. All the peaks observed can be ascribed to the pyrochlore structure, indicating that excess Er was successfully stuffed into $Er_2Ti_2O_7$. In fact, two series of diffraction peaks are observed. The first series with odd miller indices represent the pyrochlore superlattice reflections, including {1 1 1}, {3 1 1}, {3 3 1}, {5 1 1} and {5 3 1}. The second series with even miller indices, including {2 2 2}, {4 0 0}, {4 4 0}, {6 2 2} and {4 4 4}, represent the parent fluorite sublattice. It should be noted that the X-ray scattering power of oxygen is relatively small compared to that of cations [24]. Thus the XRD patterns of ETO are predominantly contributed by cations, Er and Ti. The structure of ETO is effectively tailored by the stuffing level (x). Two significant phenomena can be noted in Fig. 2: (1) the intensities of odd peaks decrease remarkably with increasing x, and (2) the peaks shift to smaller 2θ angle with increasing x, as shown in the inset of Fig. 2. Here we will discuss the effect of stuffing Er on the structure of ETO in detail.

Firstly, the intensities of pyrochlore superlattice reflections decrease with increasing stuffing level, x, whereas the intensities of peaks referred to the fluorite sublattice stay unchanged. At the maximum stuffed Er_2TiO_5 (x = 0.667), the superlattice diffraction peaks almost disappear and only the fluorite diffraction peaks remain. These observations indicate that stuffing Er eventually leads to a complete O-D structural transition: from an ordered pyrochlore structure to a disordered fluorite structure. In Er_2TiO_5, Er and Ti cations are completely randomized in the cation sublattice. During the stuffing process, the substitution of Ti by Er causes a charge imbalance due to the charge divergence of Er^{3+} and Ti^{4+}. Generally the charge compensation can be achieved by producing O vacancies, Er interstitials or Ti interstitials, without regard to electronic disorder. Theoretical calculations have proved that the reaction involving O vacancies is the most favorable mechanism [19]. Using Kröger–Vink notation, this reaction can be written as follows:

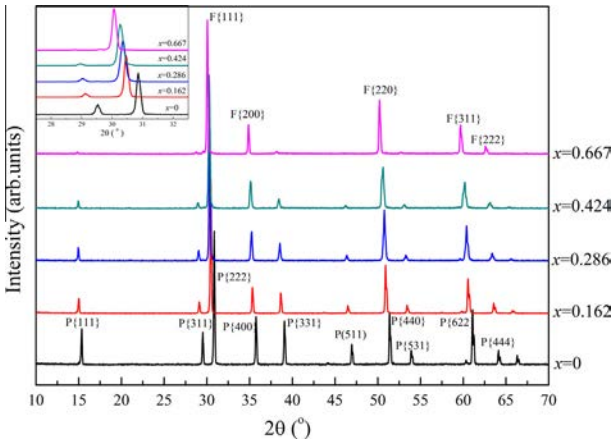

Fig. 2. XRD patterns of the pristine ETO sintered at 1500 °C. P represents the pyrochlore structure and F represents the fluorite structure. The inset presents an enlarged view of the 2θ = 27.5–32.5° region.

$$2Er_2O_3 \xrightarrow{Er_2Ti_2O_7} 2Er_{Er}^{\times} + 2Er_{Ti}' + 6O_O^{\times} + V_O^{\cdot\cdot} \quad (1)$$

According to the equation, it is clear that the O vacancies are introduced by disordering Er and Ti cations, which also leads to the disordering of anion sublattice. Commonly, the intensity ratio of an odd peak (superlattice reflection) to an even peak (fluorite structure reflection), such as I{311}/I{400}, was considered as an indicator of the ordering extent of materials. Fig. 3 (left hand) shows the calculated I{311}/I{400} of ETO samples. The value of this intensity ratio decreases almost linearly with increasing x from ~0.7 ($x = 0$) to ~0 ($x = 0.667$), suggesting the level of ordering is lowered. Similar compositionally driven O-D transition was also reported in the $Gd_2Zr_{2-x}Ti_xO_7$ and $Y_2Zr_{2-x}Ti_xO_7$ systems where the pyrochlore structure transformed to a disordered fluorite structure by the chemical substitution of Zr for Ti at B-site [21,25]. Here we also calculated the cation ratio (r_A/r_B) of ETO series. Due to the mixture of Er and Ti ions on B site in the stuffed compositions, r_B is determined by the weighted average of Er and Ti radii: $r_B = [(2-x)r_{Ti} + xr_{Er}]/2$. The results are: $r_A/r_B = 1.66$, 1.58, 1.52, 1.46 and 1.36 for $x = 0$, 0.162, 0.286, 0.424 and 0.667, respectively. According to the radius ratio criterion for $A_2B_2O_7$ pyrochlore structure ($1.46 \leqslant r_A/r_B \leqslant 1.78$), the former four compositions ($x = 0$–0.424) are pyrochlore-like and the last one ($x = 0.667$) is fluorite-like, which is consistent with the XRD results.

Secondly, the peak position shift in XRD patterns is always related to changes in the interplanar spacing of corresponding planes, and thereby, is related to changes in the lattice parameter. All the diffraction peaks shift towards smaller 2θ with increasing x, implying that the interplanar spacing of ETO lattice increases in all orientations. Based on the Bragg equation: $2d\sin\theta = \lambda$ (d is the interplanar spacing, λ is the wavelength of X-ray) and the relationship between the lattice parameter, a, and interplanar spacing in a cubic system: $a = d(h^2 + k^2 + l^2)^{1/2}$, the lattice parameters of ETO were calculated, as plotted in Fig. 3 (right hand). It is shown that the lattice parameter increases linearly with increasing x. It is worth mentioning that we take 10.24 Å as the lattice parameter for Er_2TiO_5 to present a rising tendency here. Actually, owing to the disordered fluorite structure, the lattice parameter of Er_2TiO_5 is half of this value.

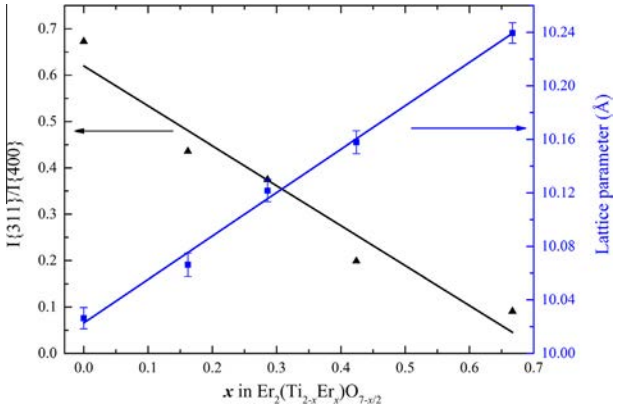

Fig. 3. Intensity ratio I{311}/I{400} (left hand) and lattice parameters (right hand) of the pristine ETO as a function of x. The error was determined as the standard deviation of lattice parameters calculated from different primary peaks.

3.2. The radiation effect of ETO

Fig. 4 shows the GIXRD patterns of the irradiated ETO samples. A series of diffraction patterns of five different compositions, before and after irradiation, are presented for various fluences. The initial structures of ETO samples are maintained in the first irradiation stage with Ne^{2+} fluence ranging from 5×10^{14} to 1×10^{15} ions/cm^2, because there is no emergence of new peaks or disappearance of original peaks. However, some slight variations can be observed: the relative intensities of the odd peaks decrease progressively, and concurrently, the diffraction peaks shift to smaller 2θ. These phenomena are particularly similar with those induced by stuffing Er as discussed above, suggesting that Ne^{2+} irradiation also leads to disordering process and lattice swelling effect in ETO. The disordering process includes: order-to-disorder transition for composition of $x = 0$ and lower-disordering state to higher-disordering state transition for compositions of $x > 0$ (since these compositions already exhibit disorder to some extent before the irradiation).

Now we consider the shift of the diffraction peaks with increasing Ne^{2+} fluence. As analyzed above, the diffraction peak shift to smaller 2θ means that Ne^{2+} irradiation induced a noticeable increase in the lattice parameter of ETO samples. To complete a

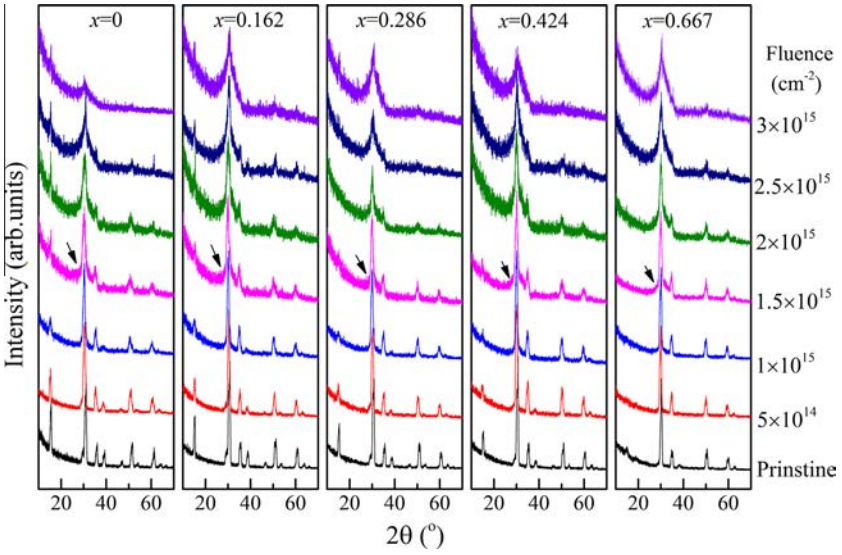

Fig. 4. GIXRD patterns of pristine and irradiated ETO ($x = 0$–0.667). The diffuse scattering indicative of partial amorphization is noted with arrows.

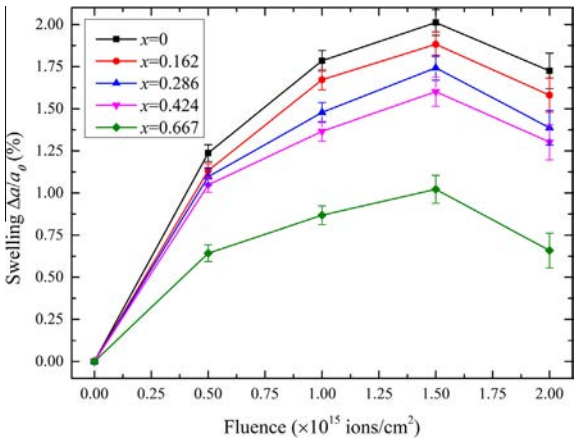

Fig. 5. Lattice swelling percentage of ETO as a function of irradiation fluence. The error was determined through the same approach as in Fig. 3.

quantitative analysis, the lattice swelling percentages $\Delta a/a_0$ (a_0 is the lattice parameter of the pristine sample) were calculated as a function of irradiation fluence for each composition and plotted in Fig. 5. The lattice parameters of all compositions increase to the maximum as the Ne^{2+} ion fluence increases to 1.5×10^{15} ions/cm^2 under which the samples become partially amorphous, and then decrease with further increase of Ne^{2+} ion fluence. Li et al. have performed a detailed study on the pre-amorphization swelling effect of $Lu_2Ti_2O_7$ [14,15,26]. The results indicate that the lattice swelling effect induced by ion irradiation in pyrochlores is primarily due to cation antisite defects. It is found in present experiments that the lattice swelling process proceeds simultaneously with the structural disordering process. Both the extent of lattice swelling and the lattice disorder of ETO increase with increasing irradiation fluence before amorphization, which confirms the role of cation antisite defects in irradiation induced lattice swelling. In addition, the swelling percentage of ETO decreases as x increases, as shown in Fig. 5. Under Ne^{2+} irradiation at fluence of 1.5×10^{15} ions/cm^2, the lattice swelling percentage of non-stuffed $Er_2Ti_2O_7$ reaches almost 2%, while for the endmember Er_2TiO_5, the lattice swelled by only ~1%. These results indicate that stuffing Er can effectively moderate the radiation-induced lattice swelling effect of ETO. Otherwise, the swelling extent of the lattice decreases when partial amorphization occurs at high irradiation fluence. Our previous studies have shown this effect clearly [15,26].

Another aspect is, as the fluence increases to 1.5×10^{15} ions/cm^2, diffuse scattering (see arrows in Fig. 4) occurs at the basis of the strongest peaks (P{2 2 2} for x = 0–0.424 and F{1 1 1} for x = 0.667), suggesting that all samples become partially amorphous at this fluence. The diffuse scattering increases with increasing Ne^{2+} fluence,

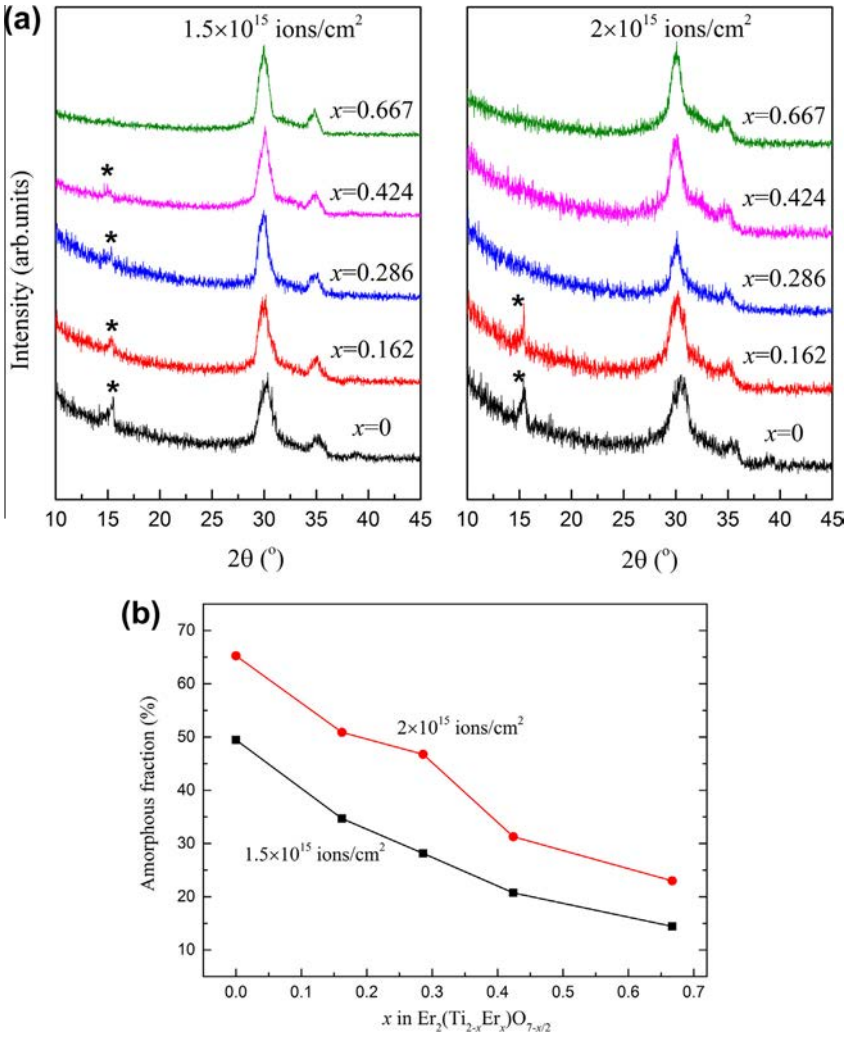

Fig. 6. (a) GIXRD patterns of irradiated ETO and (b) the calculated amorphous fraction as a function of x at fluences of 1.5×10^{15} and 2×10^{15} ions/cm^2. The visible pyrochlore superlattice diffraction peaks are marked with stars.

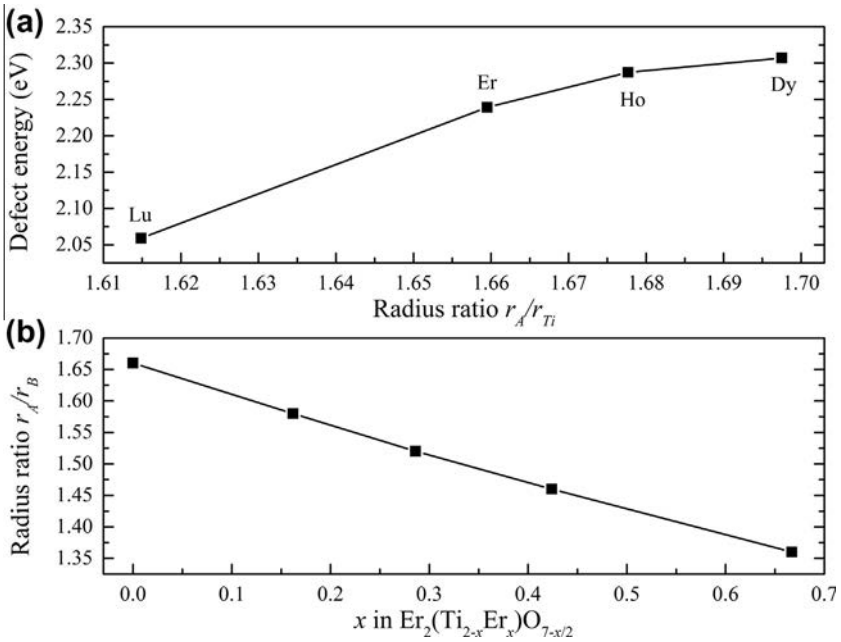

Fig. 7. (a) Cation antisite defect formation energy [28] as a function of the radius ratio r_A/r_{Ti} in $A_2Ti_2O_7$. (b) Radius ratio r_A/r_B as a function of x in ETO.

which confirms that a crystalline-to-amorphous transformation is induced by Ne ion irradiation in ETO. The amorphization process is almost complete at 3×10^{15} ions/cm^2, because the diffraction peaks from the crystalline structure have, for the most part, vanished and only the distinct diffuse scattering from the amorphous phase is detected.

For a more detailed perspective of the Ne^{2+} irradiation induced amorphization in different ETO samples, Fig. 6(a) displays the diffraction patterns of all compositions under irradiation at 1.5×10^{15} and 2×10^{15} ions/cm^2. The pyrochlore superlattice reflections (as marked with star) still exist for pyrochlore like compositions $x = 0$–0.424 at fluence of 1.5×10^{15} ions/cm^2, while, at 2×10^{15} ions/cm^2, the superlattice reflections only remained for samples of $x = 0$ and 0.162. The intensities of these peaks decrease gradually with increasing x. Meanwhile, the diffuse scattering decreases with increasing x. It appears that the compound which shows higher disordering extent is less amorphizable under irradiation. In order to facilitate a comparison among different compositions, the amorphous fraction of ETO irradiated at 1.5×10^{15} and 2×10^{15} ions/cm^2 were calculated. The XRD pattern can be decomposed into two different contributions consisting of crystalline peaks and a diffuse broad peak from the amorphous part of samples. Pseudo-Voigt profiles were used to fit these peaks. The amorphous fraction (f_a) was deduced from the ratio of the amorphous-peak area (a) to the total peak area ($a + b$, b is the area of crystalline peaks), $a/(a + b)$ [21]. Fig. 6(b) shows the calculated amorphous fraction as a function of x in ETO. On the one hand, for each composition, the amorphous fraction increases remarkably with increasing Ne fluence. On the other hand, the amorphous fraction depends strongly on the chemical compositions of ETO: the amorphous fraction decreases significantly as x increases, which is consistent for both fluences. At fluence of 2×10^{15} ions/cm^2, almost 65% of the crystalline material is amorphized for $Er_2Ti_2O_7$ ($x = 0$), while for Er_2TiO_5 ($x = 0.667$), the amorphous fraction accounts for only ~23%. Thus it is can be concluded that the compositions with smaller x are more sensitive to irradiation induced amorphization process. In other words, the radiation resistance of ETO, as measured by the remaining crystalline fraction $(1 - f_a)$, increases with increasing x.

Radiation damage processes are generally the results of defect accumulation in materials. Energy-minimization calculations suggest that cation antisite defect is the most stable defect in the pyrochlore structure and has the lowest formation energy [27,28]. In present experiments, it is expected that cation antisite defects ($Er_{Ti} + Ti_{Er}$) are produced by Ne ion irradiation, since the disordering process has been observed. The energetic Ne ions can knock the Er and Ti atoms out of their original lattice sites, which makes it possible for the two cations exchange their positions to form an antisite defect, and the defects accumulate during continued irradiation. As the local antisite defect density reaches a threshold level, an amorphous phase forms.

Further studies have stated that the cation antisite defect formation energy is closely related to the cation radius ratio, r_A/r_B. In our previous calculations of titanate pyrochlores $A_2Ti_2O_7$ (A = Dy–Lu) based on the first principle [29], the cation antisite defect energy shows a nearly linear reduction with decrease of the radius ratio, r_A/r_{Ti}, as shown in Fig. 7(a). In present work, the calculated radius ratio of A- to B-site cations, r_A/r_B, decreases with increasing x (Fig. 7(b)). As a result, the formation energy of cation antisite defect in ETO accordingly decrease as a function of x. It has been revealed that the variation trend of the formation energy of cation antisite defect is in excellent agreement with the trend of radiation resistant behavior of titanate pyrochlores [29,30]. The compound with the less antisite defect formation energy is more resistant to the irradiation induced amorphization. In this case, the increasing resistance to amorphization in ETO with increasing x is attributed to the decreasing cation antisite defect formation energy. From another point of view, Sickafus et al. have pointed out that the key to radiation tolerance is an inherent ability of accommodating atomic lattice disorder [31]. As mentioned above, the natural disordering degree of pristine ETO increases with increasing x. Hence, the resistance to ion-induced amorphization is expected to increase with increasing x.

4. Conclusions

In summary, we have investigated the structures of Er-stuffed ETO series and their microstructural evolution induced by

400 keV Ne^{2+} ion irradiation. The pristine and irradiated ETO samples were characterized by GIXRD measurement. The results suggest that stuffing Er and Ne ion irradiation have similar effects on the structural evolution of $Er_2Ti_2O_7$. Both of them induce structural disordering and lattice swelling, except that the irradiation can induce amorphization while stuffing Er cannot. For the pristine samples, the lattice parameter and disordering degree increase with increasing Er stuffing level (x). The endmember Er_2TiO_5 ($x = 0.667$) possesses a disordered fluorite structure.

Ne^{2+} ion irradiation has induced significant microstructural evolutions in ETO series, including disordering process, lattice swelling and amorphization. The lattice swelling occurs prior to the amorphization. Both lattice swelling and amorphization are correlated with the formation of cation antisite defects which also contribute to the disordering process in the irradiated samples. The stuffing level parameter, x, plays an important role in determining the radiation behavior of ETO. The compositions with larger x are more resistant to Ne^{2+} irradiation induced lattice swelling as well as amorphization. Stuffing Er has proven to be an efficient method to moderate the radiation damage in ETO.

Acknowledgements

This work was sponsored by the National Natural Science Foundation of China with Grant Nos. 11175076, 11135002 and 11475076. Ion Beam Materials Laboratory was partially supported by the Center for Integrated Nanotechnologies, a DOE nanoscience user facility jointly operated by Los Alamos and Sandia National Laboratories.

References

[1] R.C. Ewing, W.J. Weber, J. Lian, Nuclear waste disposal—pyrochlore ($A_2B_2O_7$): nuclear waste form for the immobilization of plutonium and "minor" actinides, J. Appl. Phys. 95 (2004) 5949–5971. http://scitation.aip.org/content/aip/journal/jap/95/11/10.1063/1.1707213.

[2] W.J. Weber, R.C. Ewing, C. Catlow, T.D. De La Rubia, L. Hobbs, C. Kinoshita, H. Matzke, A. Motta, M. Nastasi, E. Salje, Radiation effects in crystalline ceramics for the immobilization of high-level nuclear waste and plutonium, J. Mater. Res. 13 (1998) 1434–1484. http://journals.cambridge.org/action/displayAbstract?fromPage=online&aid=7989601&fileId=S0884291400044411.

[3] L. Shcherbakova, L. Mamsurova, G. Sukhanova, Lanthanide titanates, Russ. Chem. Rev. 48 (1979) 228. http://iopscience.iop.org/0036-021X/48/3/R02.

[4] M. Subramanian, G. Aravamudan, G. Subba Rao, Oxide pyrochlores—a review, Prog. Solid State Chem. 15 (1983) 55–143. http://www.sciencedirect.com/science/article/pii/0079678683900018.

[5] K.E. Sickafus, J.A. Valdez, J.R. Williams, R.W. Grimes, H.T. Hawkins, Radiation induced amorphization resistance in A_2O_3–BO_2 oxides, Nucl. Instr. Meth. B 191 (2002) 549–558. http://www.sciencedirect.com/science/article/pii/S0168583X02006092.

[6] J. Lian, J. Chen, L. Wang, R.C. Ewing, J.M. Farmer, L.A. Boatner, K. Helean, Radiation-induced amorphization of rare-earth titanate pyrochlores, Phys. Rev. B 68 (2003) 134107. http://journals.aps.org/prb/abstract/10.1103/PhysRevB.68.134107.

[7] J. Lian, L. Wang, J. Chen, K. Sun, R. Ewing, J. Matt Farmer, L. Boatner, The order-disorder transition in ion-irradiated pyrochlore, Acta Mater. 51 (2003) 1493–1502. http://www.sciencedirect.com/science/article/pii/S135964540200544X.

[8] F. Zhang, S. Saxena, Structural changes and pressure-induced amorphization in rare earth titanates $RE_2Ti_2O_7$ (RE: Gd, Sm) with pyrochlore structure, Chem. Phys. Lett. 413 (2005) 248–251. http://www.sciencedirect.com/science/article/pii/S0009261405011188.

[9] M. Lang, F. Zhang, J. Zhang, J. Wang, J. Lian, W.J. Weber, B. Schuster, C. Trautmann, R. Neumann, R.C. Ewing, Review of $A_2B_2O_7$ pyrochlore response to irradiation and pressure, Nucl. Instr. Meth. B 268 (2010) 2951–2959. http://www.sciencedirect.com/science/article/pii/S0168583X10004349.

[10] G. Sattonnay, S. Moll, L. Thomé, C. Legros, M. Herbst-Ghysel, F. Garrido, J.-M. Costantini, C. Trautmann, Heavy-ion irradiation of pyrochlore oxides: comparison between low and high energy regimes, Nucl. Instr. Meth. B 266 (2008) 3043–3047. http://www.sciencedirect.com/science/article/pii/S0168583X08004436.

[11] G. Sattonnay, N. Sellami, L. Thomé, C. Legros, C. Grygiel, I. Monnet, J. Jagielski, I. Jozwik-Biala, P. Simon, Structural stability of $Nd_2Zr_2O_7$ pyrochlore ion-irradiated in a broad energy range, Acta Mater. 61 (2013) 6492–6505. http://www.sciencedirect.com/science/article/pii/S1359645413005478.

[12] S. Park, M. Lang, C.L. Tracy, J. Zhang, F. Zhang, C. Trautmann, P. Kluth, M.D. Rodriguez, R.C. Ewing, Swift heavy ion irradiation-induced amorphization of $La_2Ti_2O_7$, Nucl. Instr. Meth. B 326 (2014) 145–149. http://www.sciencedirect.com/science/article/pii/S0168583X14001591.

[13] J. Lian, X. Zu, K.G. Kutty, J. Chen, L. Wang, R. Ewing, Ion-irradiation-induced amorphization of $La_2Zr_2O_7$ pyrochlore, Phys. Rev. B 66 (2002) 054108. http://journals.aps.org/prb/abstract/10.1103/PhysRevB.66.054108.

[14] Y. Li, B. Uberuaga, C. Jiang, S. Choudhury, J. Valdez, M. Patel, J. Won, Y.-Q. Wang, M. Tang, D. Safarik, Role of antisite disorder on preamorphization swelling in titanate pyrochlores, Phys. Rev. Lett. 108 (2012) 195504. http://journals.aps.org/prl/abstract/10.1103/PhysRevLett.108.195504.

[15] Y. Li, Y. Wang, C. Xu, J. Valdez, M. Tang, K. Sickafus, Microstructural evolution of the pyrochlore compound $Er_2Ti_2O_7$ induced by light ion irradiations, Nucl. Instr. Meth. B 286 (2012) 218–222. http://www.sciencedirect.com/science/article/pii/S0168583X11011530.

[16] J. Pruneda, E. Artacho, First-principles study of structural, elastic, and bonding properties of pyrochlores, Phys. Rev. B 72 (2005) 085107. http://journals.aps.org/prb/abstract/10.1103/PhysRevB.72.085107.

[17] A. Chartier, G. Catillon, J.-P. Crocombette, Key role of the cation interstitial structure in the radiation resistance of pyrochlores, Phys. Rev. Lett. 102 (2009) 155503. http://journals.aps.org/prl/abstract/10.1103/PhysRevLett.102.155503.

[18] M. Petrova, A. Novikova, R. Grebenshchikov, Phase equilibria in the Er_2O_3–TiO_2 system, (1979).

[19] C.R. Stanek, L. Minervini, R.W. Grimes, Nonstoichiometry in $A_2B_2O_7$ pyrochlores, J. Am. Ceram. Soc. 85 (2002) 2792–2798. http://onlinelibrary.wiley.com/doi/10.1111/j.1151-2916.2002.tb00530.x/abstract.

[20] M. Lang, J. Lian, J. Zhang, F. Zhang, W.J. Weber, C. Trautmann, R.C. Ewing, Single-ion tracks in $Gd_2Zr_{2-x}Ti_xO_7$ pyrochlores irradiated with swift heavy ions, Phys. Rev. B 79 (2009) 224105. http://journals.aps.org/prb/abstract/10.1103/PhysRevB.79.224105.

[21] M. Lang, F. Zhang, R. Ewing, J. Lian, C. Trautmann, Z. Wang, Structural modifications of $Gd_2Zr_{2-x}Ti_xO_7$ pyrochlore induced by swift heavy ions: disordering and amorphization, J. Mater. Res. 24 (2009) 1322–1334. http://journals.cambridge.org/action/displayAbstract?fromPage=online&aid=7949293&fileId=S0884291400032544.

[22] J.F. Ziegler, J. Biersack, U. Littmark, The Stopping and Range of Ions in Solids, New York 1985. http://link.springer.com/chapter/10.1007/978-3-642-68779-2_5?no-access=true.

[23] J.A. Valdez, Z. Chi, K.E. Sickafus, Light ion irradiation-induced phase transformation in the monoclinic polymorph of zirconia, J. Nucl. Mater. 381 (2008) 259–266. http://www.sciencedirect.com/science/article/pii/S0022311508004467.

[24] G. Lau, R. Freitas, B. Ueland, M. Dahlberg, Q. Huang, H. Zandbergen, P. Schiffer, R. Cava, Structural disorder and properties of the stuffed pyrochlore Ho_2TiO_5, Phys. Rev. B 76 (2007) 054430. http://journals.aps.org/prb/abstract/10.1103/PhysRevB.76.054430.

[25] C. Heremans, B.J. Wuensch, J.K. Stalick, E. Prince, Fast-ion conducting $Y_2(Zr_yTi_{1-y})_2O_7$ pyrochlores: neutron rietveld analysis of disorder induced by Zr substitution, J. Solid State Chem. 117 (1995) 108–121. http://www.sciencedirect.com/science/article/pii/S0022459685712534.

[26] L. Yu-Hong, X. Chun-Ping, G. Chao, W. Zhi-Guang, Ne^{2+} ion irradiation induced swelling effects in pyrochlore $Ho_2Ti_2O_7$ by using a GIXRD technique, Chin. Phys. Lett. 28 (2011) 066102. http://iopscience.iop.org/0256-307X/28/6/066102.

[27] L. Minervini, R.W. Grimes, K.E. Sickafus, Disorder in pyrochlore oxides, J. Am. Ceram. Soc. 83 (2000) 1873–1878. http://onlinelibrary.wiley.com/doi/10.1111/j.1151-2916.2000.tb01484.x/abstract.

[28] A. Chartier, C. Meis, W.J. Weber, L.R. Corrales, Theoretical study of disorder in Ti-substituted $La_2Zr_2O_7$, Phys. Rev. B 65 (2002) 134116. http://journals.aps.org/prb/abstract/10.1103/PhysRevB.65.134116.

[29] L. Chen, X. Su, Y. Li, First-principles study on cation-antisite defects of stannate and titanate pyrochlores, Open Access Libr. J. 1 (2014). http://www.oalib.com/articles/3064375#.VPAtMGMZMsY.

[30] Z.L. Zhang, H.Y. Xiao, X.T. Zu, F. Gao, W.J. Weber, First-principles calculation of structural and energetic properties for $A_2Ti_2O_7$ (A = Lu, Er, Y, Gd, Sm, Nd, La), J. Mater. Res. 24 (2009) 1335–1341. http://journals.cambridge.org/action/displayAbstract?fromPage=online&aid=7949302&fileId=S0884291400032556.

[31] K.E. Sickafus, R.W. Grimes, J.A. Valdez, A. Cleave, M. Tang, M. Ishimaru, S.M. Corish, C.R. Stanek, B.P. Uberuaga, Radiation-induced amorphization resistance and radiation tolerance in structurally related oxides, Nat. Mater. 6 (2007) 217–223. http://www.nature.com/nmat/journal/v6/n3/abs/nmat1842.html.